Escherichia coli membrane microdomain SPFH protein HflC interacts with YajC and contributes to aminoglycoside and oxidative stress tolerance

Aimee K. WESSEL[1†], Yutaka YOSHII[1†], Alexander REDER[2], Rym BOUDJEMAA[3], Magdalena SZCZESNA[1,6], Jean-Michel BETTON[4], Joaquin BERNAL-BAYARD[1,7], Christophe BELOIN[1], Daniel LOPEZ[5], Uwe VÖLKER[2], Jean-Marc GHIGO[1*]

[1] *Institut Pasteur, Université de Paris-Cité, CNRS UMR6047, Genetics of Biofilms Laboratory F-75015 Paris, France.*

[2] *Department of Functional Genomics, Interfaculty Institute for Genetics and Functional Genomics, University Medicine Greifswald, 17487 Greifswald, Germany.*

3 Abbelight, 191 avenue Aristide Briand, 94230 Cachan

[4] *Institut Pasteur, Université de Paris-Cité,, UMR UMR6047, Stress adaptation and metabolism in enterobacteria 75015 Paris, France.*

[5] *Universidad Autonoma de Madrid, Centro Nacional de Biotecnologia, Campus de Cantoblanco, Calle Darwin 3, 28049 Madrid, España*

[6] *MRC Centre for Molecular Bacteriology and Infection, Imperial College London, Armstrong Road, London SW7 2AZ, UK*

[7] *Departamento de Genética, Facultad de Biología, Universidad de Sevilla, Apartado 1095, 41080 Sevilla, Spain*

† AW and YY equally contributed to this work.

[*]**Corresponding author:** Jean-Marc Ghigo (jean-marc.ghigo@pasteur.fr)

Short Title: *E. coli* SPFH lipid raft proteins contribute to tobramycin and paraquat tolerance

Keywords

Lipid raft; membrane micro-domains; SPFH; Flotilin; Stress tolerance; *Escherichia coli*

ABSTRACT

Eukaryotic cells segregate many membrane-dependent functions into membrane microdomains also known as lipid rafts. These domains are enriched in polyisoprenoid lipids and in scaffolding proteins belonging to the Stomatin, Prohibitin, Flotillin, and HflK/C (SPFH) protein superfamily, which are also found in prokaryotes. Whereas Gram-positive bacteria were also shown to possess functional membrane microdomains (FMMs) structurally and functionally similar to eukaryotic lipid rafts, little is still known about Gram-negative bacteria FMMs. *Escherichia coli* K12 possesses 4 SPFH proteins, YqiK, QmcA, HflK, and HflC, previously shown to localize in discrete polar or lateral inner-membrane locations, raising the possibility that *E. coli* SPFH proteins could contribute to the assembly of inner-membrane FMMs regulating cellular processes.

Here we studied the determinants of the native, chromosomal QmcA and HflC cell localization using a domain swap analysis and fluorescent and super-resolution microscopy. We showed that full QmcA and HflC protein is required for achieving their native inner-membrane localization and that impairing the synthesis of cardiolipin and isoprenoid lipids known to associate with FMMs alters QmcA and HflC localization pattern. Finally, using Biolog phenotypic arrays, we showed that a mutant lacking all SPFH genes displayed increased sensitivity to aminoglycosides and oxidative stress. This phenotype is exclusively due to the absence of HflKC and a cross-linking and mass spectrometry analysis showed that YajC, a SecDF translocon accessory protein, interacts with HflC and also contributes to *E. coli* stress tolerance. Our study therefore provides insights into the function and interactions associated with SPFH proteins in *E. coli* FMMs.

IMPORTANCE

Eukaryotic cells segregate many cellular processes in cholesterol-rich functional membrane micro-domain also called lipid rafts, which contain proteins of the Stomatin, Prohibitin, Flotillin, and HflK/C (SPFH) superfamily. Whereas SPFH proteins are also present in bacteria, they were mostly studied in Gram-positive bacteria and less is known on the function of SPFH proteins in Gram-negative bacteria. Here, we showed that the cell localization of the *E. coli* SPFH proteins QmcA and HflKC is altered in absence of cardiolipin and isoprenoid lipid synthesis, suggesting that these lipids could contribute to *E. coli* membrane microdomain assembly. Using a broad phenotypic analysis and cross-linking coupled with spectrometry approaches, we identified that YajC, a SecDF-YajC translocon accessory protein, interacts with HflC and that both proteins contribute to *E. coli* tolerance to aminoglycosides and oxidative stress. Our study, therefore, provides new insights into the cellular processes associated with SPFH proteins in *E. coli* functional membrane microdomains.

INTRODUCTION

In addition to separating the intracellular content of cells from the environment, lipid bilayer membranes also contribute to specialized functions, including cross-membrane transport, enzymatic activity, signaling as well as anchoring of cytoskeletal and extracellular structures (1, 2). In eukaryotes, these membrane-dependent functions are spatially and temporally regulated by membrane microdomains called lipid rafts (3-5), broadly defined as cholesterol- and sphingolipid-enriched membrane regions formed upon lipid-lipid, lipid-protein and protein-protein interactions that compartmentalize membrane cellular processes (5-7). The Stomatin/Prohibitin/Flotillin/HflK/C (or SPFH) family of membrane proteins has been shown to localize in eukaryotic lipid rafts and to recruit and provide a stabilizing scaffold to other lipid raft-associated proteins (8-13).

Although sphingolipids and cholesterol are absent from most prokaryotes (14), the Gram-positive bacteria *Bacillus subtilis* and *Staphylococcus aureus* can also compartmentalize cellular processes in functional membrane microdomains (FMMs) (14-16). Analogous to eukaryote lipid rafts, bacterial FMMs display a distinct lipidic composition and are enriched in farnesol, hopanoids and other polyisoprenoid lipids (14, 16, 17). They also contain SPFH proteins, including flotillins, and a pool of proteins involved in diverse cellular processes (14, 16). In *B. subtilis*, flotillins FloT and FloA colocalize in membrane foci and contribute to the assembly of membrane protein complexes (18-21). Lack of flotillins impairs biofilm formation, sporulation, protease secretion, motility, and natural competence, indicating that the formation of FMMs also plays critical cellular roles in *B. subtilis* (15, 18, 22-25).

SPFH proteins are also found in Gram-negative bacteria and *Escherichia coli* K12 possesses four genes, *yqiK*, *qmcA*, *hflK*, and *hflC*, which encode proteins with a SPFH domain and a N-terminal transmembrane segment (26). QmcA and YqiK are predicted to face the cytoplasmic compartment, while HflK and HflC are predicted to be exposed in the periplasm, forming the HflKC complex negatively regulating the protease activity of FtsH against membrane proteins (27-30). HflC and QmcA are detected in *E. coli* membrane fractions resistant to solubilization by non-ionic detergents (detergent-resistant membranes or DRM) that are often used as - debatable - proxies for FMMs (31-34). Moreover, fluorescent microscopy showed that *E. coli* SPFH proteins HflC and QmcA

are localized in discrete polar or lateral membrane foci (35). This raised the possibility that *E. coli* SPFH proteins could localize in inner-membrane FMMs and regulate important cellular processes (36). However, apart from the functional and structural description of HflKC as a regulator of the FtsH membrane protease (27, 30, 37) and a recent study suggesting that YqiK is involved in cell motility and resistance to ampicillin (38), the functions of FMM in *E. coli* and other Gram negative bacteria are still poorly understood.

In this study, we used fluorescent and super resolution microscopy to perform a detailed analysis of QmcA and HflC membrane localization signals. We then showed that integrity of QmcA and HflC protein domains is required for their inner membrane localization, and that the lack of cardiolipin and isoprenoid lipids known to associate with FMMs alters their localization. Moreover, using single and multiple SPFH gene mutants, we showed that the absence of HflKC increases sensitivity to aminoglycosides and oxidative stress. Finally, cross-linking and mass spectrometry analysis allowed us to identify YajC, a protein of unknown function and an accessory component of the SecDF-YajC translocon, as a new partner that interacts and colocalizes with HflC at the cell pole and contributes to stress tolerance Our study therefore provides new insights into the function and interactions associated with *E. coli* SPFH proteins.

RESULTS

Chromosomal *E. coli* SPFH fluorescent fusion proteins show distinct localization patterns.

To investigate the determinant of cell localization of *E. coli* SPFH proteins, we first tagged YqiK and QmcA, which C-termini are predicted to be in the cytoplasm (29), with a C-terminal monomeric super folder green fluorescent protein (msfGFP). We then tagged HflC and HflK, which C-termini are predicted to be in the periplasm (29), with the C-terminal red fluorescent protein mCherry. All these fusions were expressed under their own promoter from their native chromosomal location (Sup. Fig. S1). Epifluorescence and super-resolution microscopy confirmed the previously reported polar localization of HflK and HflC (35) (Fig. 1 and Sup. Fig. S2), with 94% and 91% polar localization pattern for HflC-mCherry and HflK-mCherry, respectively (n=150). By contrast, C-terminally tagged QmcA-GFP localized exclusively as punctate distributed throughout the cell body, with 96% of the cells harboring 5 foci or more (n=150) (Fig. 1CD). However, we could not detect YqiK-GFP, possibly due to its low native chromosomal expression level. We then used anti-GFP or mCherry antibodies to perform immunodetection on cytoplasmic as well as inner and outer membrane fractions of *E. coli* strains expressing either HflC-mCherry or QmcA-GFP. In agreement with previous results (29, 36), both fusion proteins were detected in the inner membrane fraction (Fig. 2).

Domain swap analysis shows that protein integrity is essential for QmcA-GFP and HflC-mCherry localization.

To identify HflC and QmcA membrane localization signals, we constructed multiple fluorescently tagged truncated version of both proteins. We tagged with msfGFP a QmcA protein reduced to its transmembrane region and SPFH domain (TM^{QmcA}-$SPFH^{QmcA}$-GFP) and, separately, one reduced to the QmcA transmembrane region only (TM^{QmcA}-GFP) (Fig. 3A). To test the role of the QmcA transmembrane region, we also swapped TM^{QmcA} in the three constructions by the single-spanning TM domain of the phage coat protein Pf3 (TM^{Pf3}), which orients subsequent amino acids to the cytosol (38) (Fig. 3A). Similarly, in addition to the full length HflC-mCherry, we tagged with mCherry the HflC transmembrane region and SPFH domain (TM^{HflC}-$SPFH^{HflC}$-mCherry) and, separately,

only its TM region (TM^{HflC}-mCherry) (Fig. 3B). We also swapped the HflC TM region with the single-spanning TM region of colistin M immunity protein (TM^{Cmi}), which orients subsequent amino acids to the periplasm (39) (Fig. 3B). Epifluorescence microscopy of HflC and QmcA derivative fusions showed that in addition to full-length constructs only full-length constructs with swapped TM (TM^{Pf3}-QmcA-GFP and TM^{Cmi}-HflC-mCherry) displayed significant punctated foci or polar localization, respectively (Fig. 3AB), although at reduced frequency compared to native QmcA-GFP and HflC-mCherry. Finally, we prepared inner and outer membrane fractions of *E. coli* strains expressing each QmcA and HflC derivative and we observed that all these constructs were still mainly located in the inner membrane fraction. This indicates that, while we observed that QmcA-GFP and HflC-mChery derivatives exhibit altered cell localization, they do not exhibit significant mis-localization and remain located in the inner membrane (Sup. Fig. S3). These results therefore indicated that specific QmcA and HflC localization requires the combination of a transmembrane and full cytoplasmic (QmcA) or periplasmic (HflC) domain.

Lack of cardiolipin and isoprenoid lipid synthesis alters the cell localization of QmcA and HflC.

FMMs were previously shown to be enriched with negatively charged cardiolipins and isoprenoids, which promote the localization of polar proteins and modulation of membrane lipid fluidity (15, 22, 39-42). We first tested whether alteration of cardiolipin synthesis could cause mis-localization of *E. coli* SPFH proteins QmcA or HflKC in a mutant lacking the major cardiolipin synthases *clsABC* (43). Whereas epifluorescence microscopy analysis did not show clear alteration of QmcA-GFP punctate localization patterns in a *clsABC* mutant, single-molecule 2 and 3D super-resolution microscopy analysis showed a 3 to 10-fold reduction of the number of QmcA-GFP punctates compared to WT (Fig. 4A and Sup. Fig. S4). Super-resolution microscopy analysis of HflC-mCherry localization showed a drastic loss of polar localization pattern (Fig. 4B and Supp. Fig. S4). We then used an *idi* mutant unable to synthesize isoprenoid lipids due to the lack of isomerization of isopentenyl diphosphate (IPP) into dimethylallyl diphosphate (DMAPP) (44). We observed that, whereas QmcA-GFP punctate localization is not affected, HflC-mCherry polar localization was reduced in the Δ*idi*

mutant (Fig. 4A and Sup. Fig. S4). These results demonstrate that the modulation of membrane lipid fluidity alters FMM protein localization in *E. coli*.

Phenotypic analysis of *E. coli* SPFH mutant shows that only absence of HflKC increases *E. coli* sensitivity to aminoglycosides and oxidative stress.

To identify potential phenotypes and functions associated with the *E. coli* SPFH proteins YqiK, QmcA, HflK and HflC, we introduced single and multiple deletions of the corresponding SPFH genes and observed that neither single mutants nor the quadruple Δ*hflK,* Δ*hflC,* Δ*qmcA*, and Δ*yqiK* (hereafter referred to Δ*SPFH* mutant) displayed any significant growth defects in rich or minimal media (Fig. 5A and Sup. Fig. S5A). Considering the role of SPFH proteins in activation of inner-membrane kinases involved in *B. subtilis* biofilm formation (15), we tested adhesion and biofilm capacity of WT and ΔSPFH strains but could not detect any significant differences between these two strains. We then used Biolog™ phenotypic microarrays to perform a large-scale phenotypic assay comparing an *E. coli* WT and Δ*SPFH* mutant, (Sup. Table S1). This analysis revealed that the Δ*SPFH* mutant is metabolically less active when grown in the presence of various aminoglycosides (tobramycin, capreomycin, sisomicin and paromomycin) or when exposed to paraquat (Fig. 5B and Sup. Fig. S5BC). Consistently, the minimal inhibitory concentration (MIC) for tobramycin of the Δ*SPFH* mutant was 3-fold lower than that of the WT MIC (Fig.5C) and the sensitivity of the Δ*SPFH* mutant to paraquat was increased compared to the WT (Fig. 5D and Sup. Fig. S5D). Test of individual SPFH-gene mutants for their sensitivity to tobramycin and paraquat showed that the HflKC complex is the sole responsible for both phenotypes, as both single *hflK* and *hflC* or a double *hflKC* mutants displayed increased sensitivity to tobramycin and oxidative stress (Fig. 5CD and Sup. Fig. S5E). This phenotype could be complemented upon introduction of a plasmid expressing *hflKC* genes in the double *hflKC* mutant (Sup. Fig. S6A). Finally, whereas an Δ*idi* mutant showed no significant difference compared to the WT, the MIC for tobramycin and paraquat of a Δ*clsABC* mutant was reduced by 2 to 3-fold, consistent with the impact of a *cls* mutation on HflC localization (Fig. 4BD and Fig.5CD).

YajC interacts and colocalizes with HflC and contributes to tobramycin and paraquat tolerance

Considering the scaffolding role of HflKC, we hypothesized that proteins interacting with HflKC in FMMs could also contribute to tolerance to aminoglycosides and paraquat. We first tested AcrA, the efflux pump involved in the transport of a wide range of substrates including aminoglycosides (45) and YidC, an essential inner membrane protein required for proper insertion of integral inner membrane proteins (46). Both proteins were indeed previously identified in *E. coli* inner-membrane DRM fractions often biochemically associated with FMM and shown to display HflC-type pattern of polar localization when fused to fluorescent proteins and expressed from plasmids (35, 47). However, when expressed from their native chromosomal context, we could not detect any distinct AcrA-GFP nor YidC-GFP localization nor any significant co-localisation with HflC in exponential or stationary phase conditions (Sup. Fig. S7). Moreover, an *acrA* deletion did not alter *E. coli* MIC profile to tobramycin and paraquat as much as a Δ*hflC* mutant (Fig.5CD). To define additional interaction partners of HflC, we decided to use a cross-linking approach followed by affinity chromatography and mass spectrometric identification of interacting proteins. To this end, we created a translation fusion of HflC with a C-terminal double Tag consisting of a TwinStrep-Tag followed by a poly-Histidine-Tag (hereafter referred to *HflC-tag* fusion) at the native chromosomal locus. Expression of the fusion from the *hflC* promoter ensured native expression levels and minimized detection of false-positive interaction candidates due to non-physiological protein levels. Proteins were cross-linked covalently by formaldehyde treatment in quadruplicates in exponentially growing and stationary phase cells. Complexes of HflC were purified with StepTactinXT magnetic beads from both conditions and 11 or 17 possible direct interaction partners were identified by mass spectrometry in exponentially growing or stationary phase *E. coli*, respectively (Sup. Fig. S8 and Sup. Table S2 and S3). In both tested conditions, we not only identified as potential interaction partners the two well-known HflC interaction partners HflK and FtsH (27), but also YajC, a Sec translocon accessory subunit membrane protein of unknown function, and two periplasmic proteins, the thiol-reductase chaperone DsbG and the cell division coordinator of peptidoglycan synthesis CpoB (Sup. Fig. S8 and Sup Table S3).

To validate these 3 new HflC partners, we performed localization experiments for all three candidate proteins. Whereas DsbG-GFP and CpoB-GFP fusions did not display a HflC-type pattern of polar localization. (Sup. Fig. S7), we could show that YajC-GFP co-localized with HflC-mCherry at cell poles (93%; n=150) (Fig 6A). Moreover, a Δ*yajC* mutant displayed an increased sensitivity to tobramycin and paraquat (Fig 6 BC), which could be partially reverted upon complementation with a plasmid expressing *yajC* (Sup. Fig. S6AB and S8). Nevertheless, YajC-GFP polar localization was not altered in Δ*clsABC,* Δ*idi,* and Δ*hflC* mutants (Sup. Fig. S9), suggesting that YajC function or its localization are not strictly dependent on the presence of HflC. Taken together, these results indicate that the HflKC SPFH protein complex interacts with YajC and contributes to oxidative and antibiotic stress resistance.

DISCUSSION

SPFH-domain proteins have been identified in most organisms (16, 48). However, whereas SPFH-domain proteins have been extensively studied in Eukaryotes (3, 5, 49), prokaryotic SPFH proteins and proteins associated with functional membrane microdomains (FMMs) are much less understood. This is particularly the case for Gram-negative bacteria, in which potential FMMs functions are mostly inferred from studies performed in *B. subtilis* and *S. aureus*.

In this study, we investigated the functions and the localization determinants of *E. coli* SPFH proteins. We first used a domain deletion and replacement approach and showed that, although most of the tested domain replacement variants correctly localized to the inner membrane, they failed to display WT protein localization patterns. This indicates that inner-membrane localization alone is not sufficient for correct subcellular distribution of HflC and QmcA, whose localization signals might rely on multiple addressing sequences spread throughout the entirety of each protein.

The very different localization patterns of QmcA and HflKC SPFH proteins suggests that they could each be part of different FMMs, potentially using different localization signals and involved in different cellular processes. The punctate localization pattern displayed by QmcA-GFP fusion was also observed in the case of *E. coli* YqiK expressed from plasmid and of the flotillin homologues in *B. subtilis*, *S. aureus*, and *B. anthracis* flotillin homologues (15, 16, 50-52). Interestingly, *B. subtilis* and *S. aureus* flotillin genes are found associated with a gene encoding an NfeD protein, which that could contribute to protein-protein interactions within flotillin assemblies (53, 54). Consistently, like *yqiK*, *E. coli qmcA* gene is located upstream of the NfeD-like *ybbJ* gene. This further supports the notion that QmcA, like YqiK, can be considered as an *E. coli* flotillin. By contrast, the *hflKC* transcription unit lacks a downstream *nfeD* gene, suggesting that HflKC may not be a *bona fide* flotillin. However, while QmcA and YqiK have opposite orientation to HflK and HflC, they are structurally similar proteins and the four *E. coli* SPFH proteins could therefore share some degrees of functionalities. The topological similarity between HflK and HflC might contribute to HflKC complex formation and its interaction with

FtsH protease, resulting in a large periplasmic FtsH-HflKC complex localized at the cell pole (27, 28, 55-57).

The strong negative impact of QmcA or HflC transmembrane (TM) domain replacement suggests that QmcA or HflC TM domains could recognize specific membrane lipid composition facilitating the recruitment of SPFH proteins at their proper cellular membrane localization. Along with phosphatidylethanolamine and phosphatidylglycerol, cardiolipins are the primary constituent components of *E. coli* membranes that concentrate into cell poles and dividing septum (58-61). It was indeed observed that the composition of *E. coli* membrane lipid at cell poles is altered in a *clsABC* cardiolipin deficient mutant, compensated by an increased amount of phosphatidylglycerol (62). Several studies reported that cardiolipin-enriched composition in membranes at cell poles influences both the localization and activity of inner membrane proteins such as respiratory chain protein complexes and the osmosensory transporter ProP (39, 40, 63-65). In this study, we showed that, similarly to ProP, HflC and QmcA localization patterns are drastically affected in a *ΔclsABC* mutant, suggesting that *E. coli* FMMs are cardiolipin-rich microdomains, in which HflKC and QmcA complexes could act as a scaffold for FMMs cargo proteins.

Isoprenoid lipds such as farnesol, carotenoids, and hopanoids are constituents of bacterial FMMs and interact with SPFH proteins and FMM-associated proteins (14). Blocking the *S. aureus* carotenoid synthetic pathway by zaragozic acid leads to flotillin mis-localization (15). Moreover, inactivation of farnesol synthesis in a *B. subtilis yisP* mutant, which is defective for production of farnesol, impairs focal localization of the FMM-associated sensor kinase KinC (15). We showed here that in *E. coli*, interfering with the *idi* isoprenoid biosynthesis pathway also strongly alters the localization of HflC. This further documents that isoprenoid lipids contribute to the formation or integrity of FMMs, possibly by altering isoprenoid-dependent membrane rigidity, as shown in *S. aureus* and *B. subtilis* FMMs (14, 66).

Our phenotypic investigation of the function of *E. coli* SPFH proteins showed that a ΔSPFH mutant displays increased susceptibility to oxidative stress and aminoglycosides, and this sensitivity was due to the absence of HflKC. The HflKC complex was previously shown to modulate the quality control proteolytic activity of FtsH by regulating the access

of misfolded membrane protein products to FtsH (27, 28, 67). *E. coli* Δ*hflK* and Δ*hflC* mutant strains were also shown to accumulate increased amounts of hydroxyl radical, suggesting that HflK and HflC could influence tolerance to aminoglycosides and oxidative stress by suppressing excessive hydroxyl radical production. Alternatively, HflK and HflC could contribute to tobramycin resistance via FtsH-dependent proteolytic activity (68) or favoring FMM formation and the assembly of membrane proteins and lipids, such as cardiolipin, involved in the transport and movement of aminoglycosides within cells and cell membranes. Consistently, several proteins associated with aminoglycosides transport were actually detected in *E. coli* DRM fractions, including proteins involved in LPS transport (LptC, G and F), phospholipid transport (MlaD, MlaE, YebT and PqiB) and several components of the AcrAB-TolC efflux pump (35), suggesting that deletion of *hflK* or *hflC* could reduce the activity of these proteins in FMMs and enhance entry of aminoglycosides. Whereas the susceptibility to aminoglycosides indeed partly relies on the AcrAB-TolC efflux pump (45, 69-71), we found that lack of the AcrA only moderately decreases the MIC to tobramycin, compared to a *hflKC* mutation.

The use of a cross-linking approach followed by mass spectrometric analysis allowed us to identify YajC as a new HflC interacting partner. YajC is described as an unknown function accessory membrane protein contributing to the association between SecA and SecYEG translocon (72-74). Consistently with its association with HflC, the deletion of *yajC* reduced sensitivity to tobramycin and paraquat, however to a greater extent than in a Δ*SPFH* or Δ*hflKC* mutants, suggesting that lack of YajC could have a muti-factorial effect on *E. coli* antibiotic and oxidative stress resistance. Interestingly, a pump component, AcrB, was shown to co-crystalize with YajC (75). Hence, HflC could play a scaffolding role, facilitating YajC interactions with the SecDF or AcrAB-TolC protein complexes. However, the polar localization of YajC was not altered by the absence of HflC, nor in a Δ*clsABC* mutant, indicating that YajC is not strictly FMM-dependent. YajC could therefore itself be a scaffolding protein and we speculate that YajC and the HflKC-FtsH complex could be interacting only when independently localizing at cell poles. There, the lack of cardiolipin could only lead to a partial defect of HflC-YajC interactions, consistent with the observed slight increased susceptibility of a Δ*clsABC* mutant for tobramycin and paraquat compared to a wild type *E. coli*.

In conclusion, the present study provides new insights into the functions of *E. coli* SPFH proteins and some of their interacting partners and further experiments will be needed to fully uncover the roles played by this intriguing family of membrane proteins in Gram-negative bacteria.

MATERIALS & METHODS

Bacterial strains and growth conditions

Bacterial strains and plasmids used in this study are described in Sup. Table S4, and further explained in Sup. Fig. S1 and Figure 3. Unless stated otherwise, all experiments were performed in lysogeny broth (LB) or M63B1 minimal medium supplemented with 0.4% glucose (M63B1.G) at 37 °C. Antibiotics were used as follows: kanamycin (50 µg/mL); chloramphenicol (25 µg/mL); ampicillin (100 µg/mL); and zeocin (50 µg/mL). All compounds were purchased from Sigma-Aldrich (St Louis, MO, USA) except for Zeocin (InvivoGen, Santa Cruz, CA, USA).

Mutant construction

Generation of mutants in E. coli: Briefly, *E. coli* deletion or insertion mutants used in this study originated either from the *E. coli* Keio collection of mutants (76) or were generated by λ-red linear recombination using pKOBEG (Cm^R) or pKOBEGA (Amp^R) plasmids (77) using primers listed in Sup. Table S5. P1vir transduction was used to transfer mutations between different strains. When required, antibiotic resistance markers flanked by two FRT sites were removed using the Flp recombinase (78). Plasmids used in this study were constructed using an isothermal assembly method, Gibson assembly (New England Biolabs, Ipswich, MA, USA) using primers listed in Sup. Table S5. The integrity of all cloned fragments, mutations, and plasmids was verified by PCR with specific primers and DNA sequencing

Construction of deletion mutants

Δ*yqiK*, Δ*qmcA*, Δ*hflK*, Δ*hflC*, Δ*clsA*, Δ*clsB*, Δ*clsC*,Δ*idi*, Δ*acrA*, Δ*cpoB* and Δ*dsbG* deletions were transfered into *E. coli* MG1655*strep* by P1vir phage transduction from the corresponding mutants in the *E. coli* BW25113 background of the Keio collection (76). The associated kanamycin marker was then removed using the Flp recombinase expressed from the plasmid pCP20 (78). (Details regarding the construction of all other strains used in this study are presented in Sup. Table S4).

Construction of GFP and mCherry fusions

See Supplementary Materials and Methods section in Supplementary Materials

Construction of complemented strains

The *hflKC* or *yajC* genes were amplified from MG1655*strep* using primers listed in Sup. Table S5 and cloned at the downstream of the IPTG-inducible promoter of a pZS*12 vector using the Gibson assembly to generate plasmids pZS*12-HflKC and pZS*12-YajC. Then, these plasmids were introduced into Δ*hflKC* and Δ*yajC* mutants, respectively, to construct complemented mutants (Sup. Table S4). A pZS*12 empty vector was also introduced into wildtype, Δ*hflKC* and Δ*yajC* mutants. Mutants harbouring these pZS*12 plasmids were incubated and used for the below experiments in the presence of IPTG (1 mM) and ampicillin.

Epifluorescence microscopy

Bacteria were incubated into 5 mL of fresh LB medium and harvested at OD_{600} 0.4 for samples in exponential phase or OD_{600} 2.0 for stationary phase. After washing twice with M63B1 medium, cells corresponding to 1 mL of the bacterial culture were pelleted by centrifugation and resuspended into 0.1 mL of M63B1 medium for exponential samples, or 1 mL of the medium for stationary samples. Ten µL aliquots of the cell suspension were immobilized on glass slides previously covered with freshly made M63B1 medium 0.8% agarose pads. Cells were observed using a ZEISS Definite focus fluorescent microscope (Carl Zeiss, Oberkochen, Germany), equipped with an oil-immersion objective lens microscope (Pln-Apo 63X/1.4 oil Ph3). GFP or mCherry fluorescence was exited with a ZEISS Colibri LED illumination system and the fluorescence signal was detected with Zeiss FS38 HE (Carl Zeiss) or Semrock HcRed filters (Semrock, Rochester, NY, USA). GFP, and mCherry fluorescence images were taken at 1000, and 2000 msec. exposure, respectively. Image processing was performed using ImageJ and Adobe Photoshop. For each tested mutant, the subcellular localization patterns of 150 randomly selected bacteria were evaluated and the frequencies were expressed as percentiles.

Super resolution microscopy

Bacteria were imaged using single-molecule localization microscopy and stochastic optical reconstruction microscopy (SMLM-STORM), using a previously described

445 method (79). Overnight cultures were fixed with PFA 4%, permeabilized with Triton
446 0,05%, and labeled with either GFP monoclonal FluoTag®-Q — Sulfo-Cyanine 5 (Cy5),
447 or RFP monoclonal FluoTag®-Q – Cy5, which are single-domain antibodies (sdAb)
448 conjugated to Cy5. Labeling was performed at 1:250 (concentration), and washing steps
449 were carried out three times using Abbelight's SMART kit buffer. For imaging,
450 Abbelight's imaging system was used with NEO software. Abbelight's module was added
451 to an Olympus IX83 with 100x TIRF objective, N.A. 1.49. We used Hamamatsu's
452 sCMOS Flash 4 camera and a 647nm 500mW Oxxius laser, with an astigmatic lens, to
453 allow for 3D imaging of the sample (80).
454
455 **Inner membrane separation**
456 *E. coli* overnight cultures were diluted into 1 L of fresh LB medium to OD_{600} of 0.02, and
457 incubated at 37°C and 180 rpm until reaching OD_{600} 0.4. Cells were harvested and washed
458 once with 10 mM HEPES (pH 7.4) and stored at -20°C for at least 1 h. Bacteria were then
459 resuspended in 10 mL of 10 mM HEPES (pH 7.4) containing 100 µL of Benzonase (3.10^4
460 U/ml) and were passed through a FRENCH press (Thermo) at 20,000 psi. The lysate was
461 centrifugated at 15,000 *g* for 15 min at 4 °C to remove cell debris, and aliquots of the
462 suspension were stored at 4 °C as the whole extract. Then, the suspension was centrifuged
463 at 100,000 *g* for 45 min at 4 °C to separate supernatant and pellets, and aliquots of the
464 supernatant were stored at 4 °C as the cytosolic and periplasmic fractions. The pellets
465 were suspended into 600 µL of cold 10 mM HEPES (pH 7.4) and homogenized by using
466 2 mL tissue grinder (Kontes Glass, Vineland, NJ, USA). Discontinuous sucrose gradients
467 with the following composition were placed into ultracentrifugation tube: bottom to top
468 0.5 mL of 2 M sucrose, 2.0 mL of 1.5M sucrose, and 1.0 mL of 0.8 M sucrose, and 500
469 µL of the homogenized samples were placed on the top of sucrose gradients. The
470 gradients were centrifuged at 100,000 *g* for 17.5 h at 4 °C. Subsequently, 400 µL of
471 aliquots were collected into 11 microtubes from top to bottom, and the samples were
472 proceeded to the immunodetection method, as described below.
473
474 **Immunodetection of inner membrane proteins**
475 Aliquots of samples were suspended in 4× Laemmli buffer (BioRad) with 2-
476 Mercaptoethanol (Sigma) and incubated for 5 min at 98 °C. The protein samples (10 µL

each) were run on 4-20 % Mini-PROTEAN TGX Stain-FreeTM precast Gels (BioRad) in 1× TGX buffer and then transferred to nitrocellulose membrane using a Trans-Blot® Turbo™ Transfer System (BioRad). Subsequently, the membranes were blocked using blocking buffer consisting of 5% skim milk in PBS with 0.05% Tween 20 (PBST) for 2 h at 4 °C with agitation. The membranes were then incubated in PBST containing 1% skim milk with first antibodies, polyclonal rabbit antiserum raised against ExbB and TolC (kindly given by Dr. Philippe Delepelaire), GFP (Invitrogen, A6455, Thermo Fisher Scientific, Indianapolis, IN, USA) and mCherry (Invitrogen, PA5-34974) at 1:20,000 overnight at 4 °C with agitation. The membranes were washed in PBST and incubated in PBST containing 1% skim milk with a secondary antibody, anti-rabbit IgG conjugated with horseradish peroxidase (Cell signaling, 7074S), at 1:10,000 for 2 h at 25 °C with agitation. After washing the excess secondary antibody, specific bands were visualized using the ECL prime detection method (GE Healthcare) and imaged with an imaging system, iBright^{TM} CL1500 (Invitrogen).

Microbial growth phenotypic analysis

A high-throughput analysis for microbial growth phenotypes using a colorimetric reaction, Phenotype MicroArrays (Biolog Inc., Hayward, CA, USA), was performed in accordance with the manufacturer's protocol. Briefly, several colonies of *E. coli* grown on LB agar were transferred in 10 mL of a mixture of Biolog IF-0a media (BioLog) and sterilized water into a sterile capped test tube. The suspension was mixed gently, and the turbidity was adjusted to achieve the appropriate transmittance using the Biolog turbidimeter (BioLog). The cell suspension was diluted with the IF-0a plus dye mix, as mentioned in the manufacturer's protocol. 100 µL of the mixture suspension was inoculated into PM plates 1-3 and 9-20 and incubated for 72 h at 37 °C. The absorbance of each well was taken every 15 min. The OmniLog software (BioLog) was used to view and edit data, to compare data lists, and to generate reports.

Monitoring of bacterial growth

An overnight culture of *E. coli* was diluted into fresh LB and M63B1 supplemented with 0.4% glucose medium to OD_{600} of 0.05, and 200 µL aliquots were cultured in the presence or absence of paraquat (Methyl viologen dichloride hydrate, Sigma-Aldrich) in 96-well

509 microplates at 37 °C for 24 h with shaking. The absorbance of each culture at 600 nm was
510 measured every 15 min for 24 h using a microplate reader (Tecan Infinite, Mannedorf,
511 Switzerland).
512
513 **Susceptibility of *E. coli* against Tobramycin and Paraquat**
514 The broth microdilution method was used to determine the MIC (minimum inhibitory
515 concentration) values of Tobramycin (Sigma-Aldrich) and Paraquat (Sigma-Aldrich) in
516 96-well microtiter plates. Briefly, 100 µL of LB medium was distributed into each well
517 of the microtiter plates. Tobramycin was 2-fold serially diluted in each well. Five µL of
518 approximately 1×10^7 CFU/mL of *E. coli* was inoculated into each well, and the plates
519 were incubated at 37°C for 24 h. The lowest concentration that visibly inhibited bacterial
520 growth was defined as the MIC. All strains were evaluated in biological and technical
521 triplicates.
522 The spot assay was performed to evaluate the susceptibility of *E. coli* against
523 paraquat. Briefly, an overnight culture of *E. coli* was diluted into fresh LB medium to
524 OD_{600} of 0.05. Ten µL of the diluted culture was spotted on LB plates containing either
525 no or 100 µM paraquat. The plates were incubated at 37°C for 24 h, and the photographs
526 were taken. All strains were evaluated in triplicate.
527
528 **HflC-tag protein-protein interaction assay**
529
530 *Construction and growth behavior of the E. coli HflC-tag strain and growth phase*
531 *dependent expression of HflC*
532 The *hflC* gene was chromosomally tagged at its 3'end with the coding sequence for a
533 double affinity TAG, creating a translation fusion with a Twin-Strep-Tag and a 6 x His-
534 poly-histidine-Tag at the C-terminus of HflC. A 3' located kanamycin resistance cassette
535 was co-integrated with the double-Tag sequence and positive clones were selected on
536 kanamycin selective LB agar plates (50 µg/mL Km) and verified by DNA sequencing.
537 The cloning strategy and primers used for the chromosomal integration construct can be
538 found in in the Mutant construction section and Table S5. The double-affinity-Tag
539 strategy enables a two-step purification to minimize co-purification of unspecifically
540 bound proteins from the first purification step if necessary. To analyze the expression

pattern of the tagged HflC variant, the strain was cultivated in unlabeled 14N BioExpress®1000 complex medium (CGM-1000-U - Cambridge Isotope Laboratories, Inc.). Exponentially growing cells from an overnight pre-culture were used to inoculate the main culture to a starting OD_{600} of 0.05 and growth was monitored up to 2 hours after entry into stationary phase (Sup. Fig S10). Growth phase dependent expression of HflC-tag was monitored by fluorescent Western blot detection using a CW800-Cy-dye labeled StrepTactinXT conjugate on a LI-COR Odyssey CLx scanner (Sup. Fig S10). Quantification of Western blot signals with the Image Studio software (LI-COR) showed that HflC was uniformly and strongly expressed across all growth phases. To identify potential interaction partners of HflC early exponential growth phase (OD_{600} 0.4) and stationary phase (~ OD_{600} 5.5 or 1 h after entry into stat. phase) samples were selected for further testing.

$^{14}N/^{15}N$ stable isotope labeling, formaldehyde cross-linking and cell sampling

The *E. coli* wild-type strain was cultivated in both, unlabeled ^{14}N-BioExpress®1000 medium (CGM-1000-U) as well as stable isotope labeled ^{15}N-BioExpress®medium (CGM-1000-N) from Cambridge Isotope Laboratories, Inc. The *E. coli* HflC-tag strain was only cultivated in unlabeled ^{14}N-BioExpress®1000 medium. All experiments were performed in quadruplicate biological replicates. Each main culture was inoculated from exponentially growing precultures grown in the corresponding ^{14}N or ^{15}N labeled medium to a starting OD_{600} of 0.05. When the cultures reached an optical density of 0.4 or 60 min of stationary phase (~ OD_{600} 5.5) 16 OD units were either immediately harvested by centrifugation (non-crosslinked samples) or mixed with a freshly prepared Paraformaldehyde solution (4%) to a final concentration of 0.6% and incubated for 25 min at 37°C (crosslinked samples) (81, 82). The chemical cross-linking of proteins using formaldehyde has a very short cross-linking span (~2-3 Å) making it an ideal tool for detecting specific protein-protein interactions with great confidence (83). After cross-linking cells were harvested by centrifugation at room temperature for 2 min at 5000 rpm. The pellets were frozen in liquid nitrogen and stored at -80°C for further preparation.

Cell disruption and affinity Tag purification

The pellets were resuspended in 250 µL 20 mM HEPES pH 8.0 and mechanically disrupted in the frozen state using a bead mill. The powder of disrupted cells was then mixed with another 250 µL of HEPES buffer and a nuclease digestion was performed. The lysates were not centrifuged, and a protein assay (BCA) was performed from the crude lysates at a 1:50 dilution in 20mM HEPES pH8.0 with 1% SDS. For affinity purification using Strep-Tactin® Magnetic Microbeads (IBA Lifesciences GmbH, Goettingen, Germany), 750 µg of crude lysate of each sample were used and mixed with 2x concentrated wash buffer (20 mM HEPES pH 8.0 + 30% Sarcosyl) at a 1:1 volume ratio and filled up to 800 µL with 1x wash buffer (20 mM HEPES pH8.0 + 15% Sarcosyl). In parallel, 150 µL of each bead suspension was equilibrated 3 x with 1x wash buffer (equivalent to 7.5 µL beads) and the pellet was then mixed with the respective lysate (vortexed briefly) and then incubated on an overhead shaker (IKA™ Loopster Digital, Fisher scientic) at level 9 at room temperature for 1 h. Purification was then performed in the magnet rack. Samples were washed 4 times with 600 µL wash buffer and separated from the supernatants using the magnet rack. Elution was performed in 50 µL 20 mM HEPES pH 8.0 with 100 mM biotin without Sarcosyl.

SDS-PAGE, Western blot evaluation, quantification and ratio determination of $^{14}N/^{15}N$ isotope labeled purified samples

For the Western blot experiments, 4 µL of the purified eluates from exponential and stationary growth was separated by SDS-PAGE (Nu-PAGE gradient gels 4 - 12%) and transferred to a low fluorescent PVDF membrane with a BioRad Turbo Blot System (Sup. Fig S11A and B). In order to distinguish non-specifically purified and cross-linked proteins from true interaction partners, ^{14}N and ^{15}N labeled samples were mixed with respect to AccB signal intensity from the Western blots in a ratio of 1:1. Thus, the heavily labeled ^{15}N pool or reference sample was used in a constant amount of 130 ng per mass spectrometric measurement and was mixed with the corresponding volume of each ^{14}N sample of the *E. coli* wild type as well as the *E. coli* HflC-tag samples (Sup. Fig S11A and B).

Mass spectrometry and data evaluation of $^{14}N/^{15}N$ isotope labeled samples

Samples were digested and analyzed by mass spectrometry. Data were analyzed using Spectronaut 15 (directDIA, FDR = 0.01) and filtered for an ion Q-value below 0.001. Protein ratios were calculated using the median of light/heavy peptide ratios per protein. Protein ratios were then normalized using AccB ratios as reference. The statistical analysis was performed using an empirical Bayes t-test (limma package 3.50.3) (84) and multiple test adjustment utilizing the Benjamini-Hochberg approach. The criteria for significance of a potential interaction are based on an identification of the protein in at least 3 of the 4 replicates with more than 2 identified peptides per protein, a q-value below 0.05, and a calculated ratio (fold change or enrichment factor) of at least 32-fold. Proteins that were also enriched from the wildtype control, that did not contain affinity tagged proteins, represent unspecific resin interactions and were removed from the list of HflC interaction partners (Sup. Fig. S8 and Sup Table S2 and 3). Supplementary Table S6 and S7 summarize the reversed phase liquid chromatography (RPLC) as well as the mass spectrometry method used.

Statistical analysis

Data analysis was performed using GraphPad Prism 6.0 software (GraphPad, La Jolla, CA, USA). All data are expressed as mean (± standard deviation, SD) in figures. Statistical analysis was performed using Two-tailed unpaired *t-test* with Welch correction. Differences were considered statistically significant for *P* values of <0.05.

ACKNOWLEDGMENTS

We thank Philippe Delepelaire for insightful comments and material support. We are grateful to Eva Wolrab and Sven van Teeffelen for their initial interest in the project and for providing the strains for msfGFP and mCherry constructions. We thank Uwe Sauer and Philip Warmer for initial assessment of lipid composition of some of the strains used in this study. This work was supported by EU Horizon 2020 Rafts4Biotech grant 720776 (to JMG, DL, AKW, YY, AR, UV and MS), the French government's Investissement d'Avenir Program, Laboratoire d'Excellence "Integrative Biology of Emerging Infectious Diseases" (grant n°ANR-10-LABX-62-IBEID) and the *Fondation pour la Recherche Médicale* (grant no. DEQ20180339185). This work benefited from the facilities and expertise of Add Photonic BioImaging platform (UTechS PBI, Institut Pasteur). A.K.W. was supported by a Pasteur-Roux-Cantarini postdoctoral and a grant from the Philippe Foundation.

AUTHOR CONTRIBUTIONS:

A.K.W., Y.Y., and J.-M.G. designed the experiments. A.K.W., Y.Y., A.R., R.B.; M.S., J.B-B. performed the experiments. A.K.W., Y.Y., A.R., U.V. M.S., R.B., J.-M.B., C.B., D.L. and J.-M.G. analyzed the data. Y.Y., A.K.W. and J.-M.G. wrote the paper with significant contribution from all authors.

REFERENCES

1. **Alberts B, Johnson A, Lewis J, Raff M, Roberts K, Walter P.** 2002. Molecular biology of the cell 6th edition ed. Garland Science., New York.
2. **Cho W, Stahelin RV.** 2005. Membrane-protein interactions in cell signaling and membrane trafficking. Annu Rev Biophys Biomol Struct **34:**119-151.10.1146/annurev.biophys.33.110502.133337: 10.1146/annurev.biophys.33.110502.133337
3. **Simons K, Ikonen E.** 1997. Functional rafts in cell membranes. Nature **387:**569-572.10.1038/42408: 10.1038/42408
4. **Rajendran L, Simons K.** 2005. Lipid rafts and membrane dynamics. J Cell Sci **118:**1099-1102.10.1242/jcs.01681: 10.1242/jcs.01681
5. **Simons K, Sampaio JL.** 2011. Membrane organization and lipid rafts. Cold Spring Harb Perspect Biol **3:**a004697.10.1101/cshperspect.a004697: 10.1101/cshperspect.a004697
6. **Pike LJ.** 2006. Rafts defined: a report on the Keystone Symposium on Lipid Rafts and Cell Function. J Lipid Res **47:**1597-1598.10.1194/jlr.E600002-JLR200: 10.1194/jlr.E600002-JLR200
7. **Sezgin E, Levental I, Mayor S, Eggeling C.** 2017. The mystery of membrane organization: composition, regulation and roles of lipid rafts. Nat Rev Mol Cell Biol **18:**361-374.10.1038/nrm.2017.16: 10.1038/nrm.2017.16
8. **Langhorst MF, Reuter A, Stuermer CA.** 2005. Scaffolding microdomains and beyond: the function of reggie/flotillin proteins. Cell Mol Life Sci **62:**2228-2240.10.1007/s00018-005-5166-4: 10.1007/s00018-005-5166-4
9. **Morrow IC, Parton RG.** 2005. Flotillins and the PHB domain protein family: rafts, worms and anaesthetics. Traffic **6:**725-740.10.1111/j.1600-0854.2005.00318.x: 10.1111/j.1600-0854.2005.00318.x
10. **Stuermer CA, Plattner H.** 2005. The 'lipid raft' microdomain proteins reggie-1 and reggie-2 (flotillins) are scaffolds for protein interaction and signalling. Biochem Soc Symp**:**109-118.10.1042/bss0720109: 10.1042/bss0720109
11. **Browman DT, Hoegg MB, Robbins SM.** 2007. The SPFH domain-containing proteins: more than lipid raft markers. Trends Cell Biol **17:**394-402.10.1016/j.tcb.2007.06.005: 10.1016/j.tcb.2007.06.005
12. **Zeke A, Lukács M, Lim WA, Reményi A.** 2009. Scaffolds: interaction platforms for cellular signalling circuits. Trends Cell Biol **19:**364-374.10.1016/j.tcb.2009.05.007: 10.1016/j.tcb.2009.05.007
13. **Zhao F, Zhang J, Liu YS, Li L, He YL.** 2011. Research advances on flotillins. Virol J **8:**479.10.1186/1743-422x-8-479: 10.1186/1743-422x-8-479
14. **Lopez D, Koch G.** 2017. Exploring functional membrane microdomains in bacteria: an overview. Curr Opin Microbiol **36:**76-84.10.1016/j.mib.2017.02.001: 10.1016/j.mib.2017.02.001
15. **Lopez D, Kolter R.** 2010. Functional microdomains in bacterial membranes. Genes Dev **24:**1893-1902.10.1101/gad.1945010: 10.1101/gad.1945010
16. **Bramkamp M, Lopez D.** 2015. Exploring the existence of lipid rafts in bacteria. Microbiol Mol Biol Rev **79:**81-100.10.1128/mmbr.00036-14: 10.1128/mmbr.00036-14

17. **Willdigg JR, Helmann JD.** 2021. Mini Review: Bacterial Membrane Composition and Its Modulation in Response to Stress. Front Mol Biosci **8:**634438.10.3389/fmolb.2021.634438: 10.3389/fmolb.2021.634438
18. **Dempwolff F, Möller HM, Graumann PL.** 2012. Synthetic motility and cell shape defects associated with deletions of flotillin/reggie paralogs in Bacillus subtilis and interplay of these proteins with NfeD proteins. J Bacteriol **194:**4652-4661.10.1128/jb.00910-12: 10.1128/jb.00910-12
19. **Bach JN, Bramkamp M.** 2013. Flotillins functionally organize the bacterial membrane. Mol Microbiol **88:**1205-1217.10.1111/mmi.12252: 10.1111/mmi.12252
20. **Schneider J, Klein T, Mielich-Süss B, Koch G, Franke C, Kuipers OP, Kovács Á T, Sauer M, Lopez D.** 2015. Spatio-temporal remodeling of functional membrane microdomains organizes the signaling networks of a bacterium. PLoS Genet **11:**e1005140.10.1371/journal.pgen.1005140: 10.1371/journal.pgen.1005140
21. **Wagner RM, Kricks L, Lopez D.** 2017. Functional Membrane Microdomains Organize Signaling Networks in Bacteria. J Membr Biol **250:**367-378.10.1007/s00232-016-9923-0: 10.1007/s00232-016-9923-0
22. **Donovan C, Bramkamp M.** 2009. Characterization and subcellular localization of a bacterial flotillin homologue. Microbiology **155:**1786-1799.10.1099/mic.0.025312-0: 10.1099/mic.0.025312-0
23. **Yepes A, Schneider J, Mielich B, Koch G, García-Betancur JC, Ramamurthi KS, Vlamakis H, López D.** 2012. The biofilm formation defect of a Bacillus subtilis flotillin-defective mutant involves the protease FtsH. Mol Microbiol **86:**457-471.10.1111/j.1365-2958.2012.08205.x: 10.1111/j.1365-2958.2012.08205.x
24. **Mielich-Süss B, Schneider J, Lopez D.** 2013. Overproduction of flotillin influences cell differentiation and shape in Bacillus subtilis. mBio **4:**e00719-00713.10.1128/mBio.00719-13: 10.1128/mBio.00719-13
25. **Schneider J, Mielich-Süss B, Böhme R, Lopez D.** 2015. In vivo characterization of the scaffold activity of flotillin on the membrane kinase KinC of Bacillus subtilis. Microbiology **161:**1871-1887.10.1099/mic.0.000137: 10.1099/mic.0.000137
26. **Hinderhofer M, Walker CA, Friemel A, Stuermer CA, Möller HM, Reuter A.** 2009. Evolution of prokaryotic SPFH proteins. BMC Evol Biol **9:**10.10.1186/1471-2148-9-10: 10.1186/1471-2148-9-10
27. **Kihara A, Akiyama Y, Ito K.** 1996. A protease complex in the Escherichia coli plasma membrane: HflKC (HflA) forms a complex with FtsH (HflB), regulating its proteolytic activity against SecY. Embo j **15:**6122-6131
28. **Saikawa N, Akiyama Y, Ito K.** 2004. FtsH exists as an exceptionally large complex containing HflKC in the plasma membrane of Escherichia coli. J Struct Biol **146:**123-129.10.1016/j.jsb.2003.09.020: 10.1016/j.jsb.2003.09.020
29. **Chiba S, Ito K, Akiyama Y.** 2006. The Escherichia coli plasma membrane contains two PHB (prohibitin homology) domain protein complexes of opposite orientations. Mol Microbiol **60:**448-457.10.1111/j.1365-2958.2006.05104.x: 10.1111/j.1365-2958.2006.05104.x
30. **Ma C, Wang C, Luo D, Yan L, Yang W, Li N, Gao N.** 2022. Structural insights into the membrane microdomain organization by SPFH family proteins.

Cell Res **32:**176-189.10.1038/s41422-021-00598-3: 10.1038/s41422-021-00598-3

31. **Brown DA, Rose JK.** 1992. Sorting of GPI-anchored proteins to glycolipid-enriched membrane subdomains during transport to the apical cell surface. Cell **68:**533-544.10.1016/0092-8674(92)90189-j: 10.1016/0092-8674(92)90189-j
32. **Schroeder R, London E, Brown D.** 1994. Interactions between saturated acyl chains confer detergent resistance on lipids and glycosylphosphatidylinositol (GPI)-anchored proteins: GPI-anchored proteins in liposomes and cells show similar behavior. Proc Natl Acad Sci U S A **91:**12130-12134.10.1073/pnas.91.25.12130: 10.1073/pnas.91.25.12130
33. **Lichtenberg D, Goñi FM, Heerklotz H.** 2005. Detergent-resistant membranes should not be identified with membrane rafts. Trends Biochem Sci **30:**430-436.10.1016/j.tibs.2005.06.004: 10.1016/j.tibs.2005.06.004
34. **Brown DA.** 2006. Lipid rafts, detergent-resistant membranes, and raft targeting signals. Physiology (Bethesda) **21:**430-439.10.1152/physiol.00032.2006: 10.1152/physiol.00032.2006
35. **Guzmán-Flores JE, Steinemann-Hernández L, González de la Vara LE, Gavilanes-Ruiz M, Romeo T, Alvarez AF, Georgellis D.** 2019. Proteomic analysis of Escherichia coli detergent-resistant membranes (DRM). PLoS One **14:**e0223794.10.1371/journal.pone.0223794: 10.1371/journal.pone.0223794
36. **Guzman-Flores JE, Alvarez AF, Poggio S, Gavilanes-Ruiz M, Georgellis D.** 2017. Isolation of detergent-resistant membranes (DRMs) from Escherichia coli. Anal Biochem **518:**1-8.10.1016/j.ab.2016.10.025: 10.1016/j.ab.2016.10.025
37. **Ito K, Akiyama Y.** 2005. Cellular functions, mechanism of action, and regulation of FtsH protease. Annu Rev Microbiol **59:**211-231.10.1146/annurev.micro.59.030804.121316: 10.1146/annurev.micro.59.030804.121316
38. **Padilla-Vaca F, Vargas-Maya NI, Elizarrarás-Vargas NU, Rangel-Serrano Á, Cardoso-Reyes LR, Razo-Soria T, Membrillo-Hernández J, Franco B.** 2019. Flotillin homologue is involved in the swimming behavior of Escherichia coli. Arch Microbiol **201:**999-1008.10.1007/s00203-019-01670-8: 10.1007/s00203-019-01670-8
39. **Romantsov T, Helbig S, Culham DE, Gill C, Stalker L, Wood JM.** 2007. Cardiolipin promotes polar localization of osmosensory transporter ProP in Escherichia coli. Mol Microbiol **64:**1455-1465.10.1111/j.1365-2958.2007.05727.x: 10.1111/j.1365-2958.2007.05727.x
40. **Mileykovskaya E, Dowhan W.** 2009. Cardiolipin membrane domains in prokaryotes and eukaryotes. Biochim Biophys Acta **1788:**2084-2091.10.1016/j.bbamem.2009.04.003: 10.1016/j.bbamem.2009.04.003
41. **Feng X, Hu Y, Zheng Y, Zhu W, Li K, Huang CH, Ko TP, Ren F, Chan HC, Nega M, Bogue S, López D, Kolter R, Götz F, Guo RT, Oldfield E.** 2014. Structural and functional analysis of Bacillus subtilis YisP reveals a role of its product in biofilm production. Chem Biol **21:**1557-1563.10.1016/j.chembiol.2014.08.018: 10.1016/j.chembiol.2014.08.018
42. **Zielińska A, Savietto A, de Sousa Borges A, Martinez D, Berbon M, Roelofsen JR, Hartman AM, de Boer R, van der Klei IJ, Hirsch AKH, Habenstein B, Bramkamp M, Scheffers D-J.** 2020. Flotillin mediated

membrane fluidity controls peptidoglycan synthesis and MreB movement. bioRxiv**:**736819.10.1101/736819: 10.1101/736819

43. **Nishijima S, Asami Y, Uetake N, Yamagoe S, Ohta A, Shibuya I.** 1988. Disruption of the Escherichia coli cls gene responsible for cardiolipin synthesis. J Bacteriol **170:**775-780.10.1128/jb.170.2.775-780.1988: 10.1128/jb.170.2.775-780.1988

44. **Hahn FM, Hurlburt AP, Poulter CD.** 1999. Escherichia coli open reading frame 696 is idi, a nonessential gene encoding isopentenyl diphosphate isomerase. J Bacteriol **181:**4499-4504

45. **Aires JR, Nikaido H.** 2005. Aminoglycosides are captured from both periplasm and cytoplasm by the AcrD multidrug efflux transporter of Escherichia coli. J Bacteriol **187:**1923-1929.10.1128/jb.187.6.1923-1929.2005: 10.1128/jb.187.6.1923-1929.2005

46. **Samuelson JC, Chen M, Jiang F, Möller I, Wiedmann M, Kuhn A, Phillips GJ, Dalbey RE.** 2000. YidC mediates membrane protein insertion in bacteria. Nature **406:**637-641.10.1038/35020586: 10.1038/35020586

47. **Urbanus ML, Fröderberg L, Drew D, Björk P, de Gier JW, Brunner J, Oudega B, Luirink J.** 2002. Targeting, insertion, and localization of Escherichia coli YidC. J Biol Chem **277:**12718-12723.10.1074/jbc.M200311200: 10.1074/jbc.M200311200

48. **Tavernarakis N, Driscoll M, Kyrpides NC.** 1999. The SPFH domain: implicated in regulating targeted protein turnover in stomatins and other membrane-associated proteins. Trends Biochem Sci **24:**425-427.10.1016/s0968-0004(99)01467-x: 10.1016/s0968-0004(99)01467-x

49. **Morrow IC, Rea S, Martin S, Prior IA, Prohaska R, Hancock JF, James DE, Parton RG.** 2002. Flotillin-1/reggie-2 traffics to surface raft domains via a novel golgi-independent pathway. Identification of a novel membrane targeting domain and a role for palmitoylation. J Biol Chem **277:**48834-48841.10.1074/jbc.M209082200: 10.1074/jbc.M209082200

50. **Dempwolff F, Schmidt FK, Hervás AB, Stroh A, Rösch TC, Riese CN, Dersch S, Heimerl T, Lucena D, Hülsbusch N, Stuermer CA, Takeshita N, Fischer R, Eckhardt B, Graumann PL.** 2016. Super Resolution Fluorescence Microscopy and Tracking of Bacterial Flotillin (Reggie) Paralogs Provide Evidence for Defined-Sized Protein Microdomains within the Bacterial Membrane but Absence of Clusters Containing Detergent-Resistant Proteins. PLoS Genet **12:**e1006116.10.1371/journal.pgen.1006116: 10.1371/journal.pgen.1006116

51. **Somani VK, Aggarwal S, Singh D, Prasad T, Bhatnagar R.** 2016. Identification of Novel Raft Marker Protein, FlotP in Bacillus anthracis. Front Microbiol **7:**169.10.3389/fmicb.2016.00169: 10.3389/fmicb.2016.00169

52. **García-Fernández E, Koch G, Wagner RM, Fekete A, Stengel ST, Schneider J, Mielich-Süss B, Geibel S, Markert SM, Stigloher C, Lopez D.** 2017. Membrane Microdomain Disassembly Inhibits MRSA Antibiotic Resistance. Cell **171:**1354-1367.e1320.10.1016/j.cell.2017.10.012: 10.1016/j.cell.2017.10.012

53. **Dempwolff F, Wischhusen HM, Specht M, Graumann PL.** 2012. The deletion of bacterial dynamin and flotillin genes results in pleiotrophic effects on

cell division, cell growth and in cell shape maintenance. BMC Microbiol **12:**298.10.1186/1471-2180-12-298: 10.1186/1471-2180-12-298

54. **Yokoyama H, Matsui I.** 2020. The lipid raft markers stomatin, prohibitin, flotillin, and HflK/C (SPFH)-domain proteins form an operon with NfeD proteins and function with apolar polyisoprenoid lipids. Crit Rev Microbiol **46:**38-48.10.1080/1040841x.2020.1716682: 10.1080/1040841x.2020.1716682
55. **Kihara A, Ito K.** 1998. Translocation, folding, and stability of the HflKC complex with signal anchor topogenic sequences. J Biol Chem **273:**29770-29775.10.1074/jbc.273.45.29770: 10.1074/jbc.273.45.29770
56. **Edgar R, Rokney A, Feeney M, Semsey S, Kessel M, Goldberg MB, Adhya S, Oppenheim AB.** 2008. Bacteriophage infection is targeted to cellular poles. Mol Microbiol **68:**1107-1116.10.1111/j.1365-2958.2008.06205.x: 10.1111/j.1365-2958.2008.06205.x
57. **Bandyopadhyay K, Parua PK, Datta AB, Parrack P.** 2010. Escherichia coli HflK and HflC can individually inhibit the HflB (FtsH)-mediated proteolysis of lambdaCII in vitro. Arch Biochem Biophys **501:**239-243.10.1016/j.abb.2010.06.030: 10.1016/j.abb.2010.06.030
58. **Raetz CR, Dowhan W.** 1990. Biosynthesis and function of phospholipids in Escherichia coli. J Biol Chem **265:**1235-1238
59. **Lin TY, Weibel DB.** 2016. Organization and function of anionic phospholipids in bacteria. Appl Microbiol Biotechnol **100:**4255-4267.10.1007/s00253-016-7468-x: 10.1007/s00253-016-7468-x
60. **Sohlenkamp C, Geiger O.** 2016. Bacterial membrane lipids: diversity in structures and pathways. FEMS Microbiol Rev **40:**133-159.10.1093/femsre/fuv008: 10.1093/femsre/fuv008
61. **El Khoury M, Swain J, Sautrey G, Zimmermann L, Van Der Smissen P, Décout JL, Mingeot-Leclercq MP.** 2017. Targeting Bacterial Cardiolipin Enriched Microdomains: An Antimicrobial Strategy Used by Amphiphilic Aminoglycoside Antibiotics. Sci Rep **7:**10697.10.1038/s41598-017-10543-3: 10.1038/s41598-017-10543-3
62. **Oliver PM, Crooks JA, Leidl M, Yoon EJ, Saghatelian A, Weibel DB.** 2014. Localization of anionic phospholipids in Escherichia coli cells. J Bacteriol **196:**3386-3398.10.1128/jb.01877-14: 10.1128/jb.01877-14
63. **Romantsov T, Stalker L, Culham DE, Wood JM.** 2008. Cardiolipin controls the osmotic stress response and the subcellular location of transporter ProP in Escherichia coli. J Biol Chem **283:**12314-12323.10.1074/jbc.M709871200: 10.1074/jbc.M709871200
64. **Arias-Cartin R, Grimaldi S, Arnoux P, Guigliarelli B, Magalon A.** 2012. Cardiolipin binding in bacterial respiratory complexes: structural and functional implications. Biochim Biophys Acta **1817:**1937-1949.10.1016/j.bbabio.2012.04.005: 10.1016/j.bbabio.2012.04.005
65. **Romantsov T, Gonzalez K, Sahtout N, Culham DE, Coumoundouros C, Garner J, Kerr CH, Chang L, Turner RJ, Wood JM.** 2018. Cardiolipin synthase A colocalizes with cardiolipin and osmosensing transporter ProP at the poles of Escherichia coli cells. Mol Microbiol **107:**623-638.10.1111/mmi.13904: 10.1111/mmi.13904
66. **van Tilburg AY, Warmer P, van Heel AJ, Sauer U, Kuipers OP.** 2022. Membrane composition and organization of Bacillus subtilis 168 and its

883 genome-reduced derivative miniBacillus PG10. Microb Biotechnol **15:**1633-
884 1651.10.1111/1751-7915.13978: 10.1111/1751-7915.13978
885 67. **Akiyama Y.** 2009. Quality control of cytoplasmic membrane proteins in
886 Escherichia coli. J Biochem **146:**449-454.10.1093/jb/mvp071:
887 10.1093/jb/mvp071
888 68. **Hinz A, Lee S, Jacoby K, Manoil C.** 2011. Membrane proteases and
889 aminoglycoside antibiotic resistance. J Bacteriol **193:**4790-
890 4797.10.1128/jb.05133-11: 10.1128/jb.05133-11
891 69. **Venter H, Mowla R, Ohene-Agyei T, Ma S.** 2015. RND-type drug efflux
892 pumps from Gram-negative bacteria: molecular mechanism and inhibition. Front
893 Microbiol **6:**377.10.3389/fmicb.2015.00377: 10.3389/fmicb.2015.00377
894 70. **Nikaido E, Shirosaka I, Yamaguchi A, Nishino K.** 2011. Regulation of the
895 AcrAB multidrug efflux pump in Salmonella enterica serovar Typhimurium in
896 response to indole and paraquat. Microbiology **157:**648-
897 655.10.1099/mic.0.045757-0: 10.1099/mic.0.045757-0
898 71. **Garneau-Tsodikova S, Labby KJ.** 2016. Mechanisms of Resistance to
899 Aminoglycoside Antibiotics: Overview and Perspectives. Medchemcomm **7:**11-
900 27.10.1039/c5md00344j: 10.1039/c5md00344j
901 72. **Pogliano KJ, Beckwith J.** 1994. Genetic and molecular characterization of the
902 Escherichia coli secD operon and its products. J Bacteriol **176:**804-
903 814.10.1128/jb.176.3.804-814.1994: 10.1128/jb.176.3.804-814.1994
904 73. **Kato Y, Nishiyama K, Tokuda H.** 2003. Depletion of SecDF-YajC causes a
905 decrease in the level of SecG: implication for their functional interaction. FEBS
906 Lett **550:**114-118.10.1016/s0014-5793(03)00847-0: 10.1016/s0014-
907 5793(03)00847-0
908 74. **Crane JM, Randall LL.** 2017. The Sec System: Protein Export in Escherichia
909 coli. EcoSal Plus **7**.10.1128/ecosalplus.ESP-0002-2017:
910 10.1128/ecosalplus.ESP-0002-2017
911 75. **Törnroth-Horsefield S, Gourdon P, Horsefield R, Brive L, Yamamoto N,**
912 **Mori H, Snijder A, Neutze R.** 2007. Crystal structure of AcrB in complex with
913 a single transmembrane subunit reveals another twist. Structure **15:**1663-
914 1673.10.1016/j.str.2007.09.023: 10.1016/j.str.2007.09.023
915 76. **Baba T, Ara T, Hasegawa M, Takai Y, Okumura Y, Baba M, Datsenko KA,**
916 **Tomita M, Wanner BL, Mori H.** 2006. Construction of Escherichia coli K-12
917 in-frame, single-gene knockout mutants: the Keio collection. Mol Syst Biol
918 **2:**2006.0008.10.1038/msb4100050: 10.1038/msb4100050
919 77. **Chaveroche MK, Ghigo JM, d'Enfert C.** 2000. A rapid method for efficient
920 gene replacement in the filamentous fungus Aspergillus nidulans. Nucleic Acids
921 Res **28:**E97.10.1093/nar/28.22.e97: 10.1093/nar/28.22.e97
922 78. **Cherepanov PP, Wackernagel W.** 1995. Gene disruption in Escherichia coli:
923 TcR and KmR cassettes with the option of Flp-catalyzed excision of the
924 antibiotic-resistance determinant. Gene **158:**9-14.10.1016/0378-1119(95)00193-
925 a: 10.1016/0378-1119(95)00193-a
926 79. **Boudjemaa R, Cabriel C, Dubois-Brissonnet F, Bourg N, Dupuis G, Gruss**
927 **A, Leveque-Fort S, Briandet R, Fontaine-Aupart MP, Steenkeste K.** 2018.
928 Impact of Bacterial Membrane Fatty Acid Composition on the Failure of
929 Daptomycin To Kill Staphylococcus aureus. Antimicrob Agents Chemother
930 **62**.10.1128/AAC.00023-18: 10.1128/AAC.00023-18

80. **Cabriel C, Bourg N, Dupuis G, Leveque-Fort S.** 2018. Aberration-accounting calibration for 3D single-molecule localization microscopy. Opt Lett **43:**174-177.10.1364/OL.43.000174: 10.1364/OL.43.000174

81. **Herzberg C, Weidinger LA, Dörrbecker B, Hübner S, Stülke J, Commichau FM.** 2007. SPINE: a method for the rapid detection and analysis of protein-protein interactions in vivo. Proteomics **7:**4032-4035.10.1002/pmic.200700491: 10.1002/pmic.200700491

82. **Müller VS, Jungblut PR, Meyer TF, Hunke S.** 2011. Membrane-SPINE: an improved method to identify protein-protein interaction partners of membrane proteins in vivo. Proteomics **11:**2124-2128.10.1002/pmic.201000558: 10.1002/pmic.201000558

83. **Sutherland BW, Toews J, Kast J.** 2008. Utility of formaldehyde cross-linking and mass spectrometry in the study of protein-protein interactions. J Mass Spectrom **43:**699-715.10.1002/jms.1415: 10.1002/jms.1415

84. **Ritchie ME, Phipson B, Wu D, Hu Y, Law CW, Shi W, Smyth GK.** 2015. limma powers differential expression analyses for RNA-sequencing and microarray studies. Nucleic Acids Res **43:**e47.10.1093/nar/gkv007: 10.1093/nar/gkv007

950 **FIGURES**

951

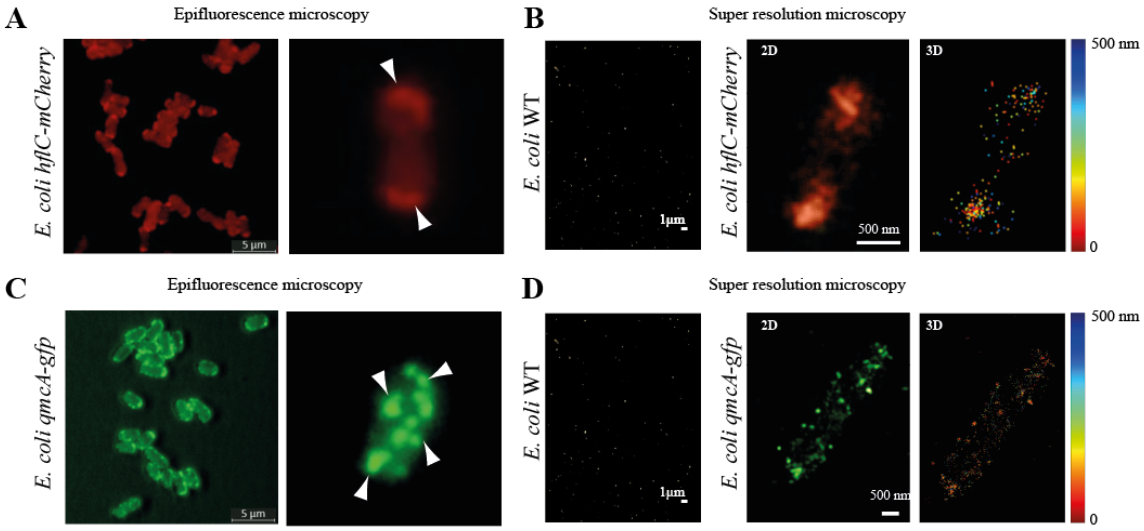

952

953 **Figure 1. Cell localization patterns of HflC and QmcA. A** and **C**: Epifluorescence
954 microscopy of cells expressing HflC-mCherry (A) or QmcA-GFP (C). Arrowheads
955 indicate polar or punctate localization foci. **B** and **D**: Super-resolution microscopy of cells
956 expressing HflC-mCherry (B) or QmcA-GFP (D). *Left panels*: lack of subcellular
957 localization in WT cells. *Center panels*: 3D images-artificial colors (red for HflC-
958 mCherry, green for QmcA-gfp). *Right panels*: 3D localization of HflC-mCherry and
959 QmcA-GFP, with colors corresponding to depth location along the Z axis, 0-500 nm, with
960 0 nm expressed in red, and 500 nm expressed in deep blue. Scales are indicated as white
961 bars.

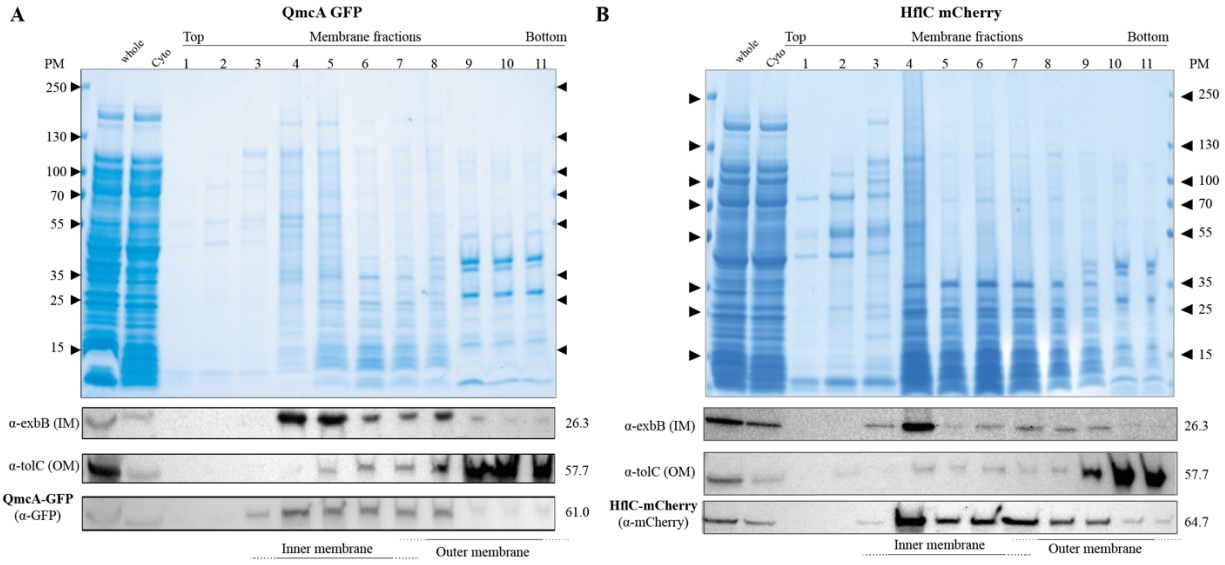

962
963

964 **Figure 2. QmcA and HflC localize to the inner membrane.** SDS-PAGE and
965 immunodetection analyses of whole-cell extracts, cytosolic fractions, and inner (IM) or
966 outer membrane (OM) fractions prepared from cells expressing QmcA-GFP (**A**) and
967 HflC-mCherry (**B**). Anti-GFP and anti-mCherry antibodies were used to detect the
968 presence of QmcA-GFP and HflC-mCherry, respectively. An anti-ExbB antibody were
969 used to detect the inner membrane- (IM) marker ExbB and anti-TolC antibodies to detect
970 the outer membrane- (OM) marker TolC.

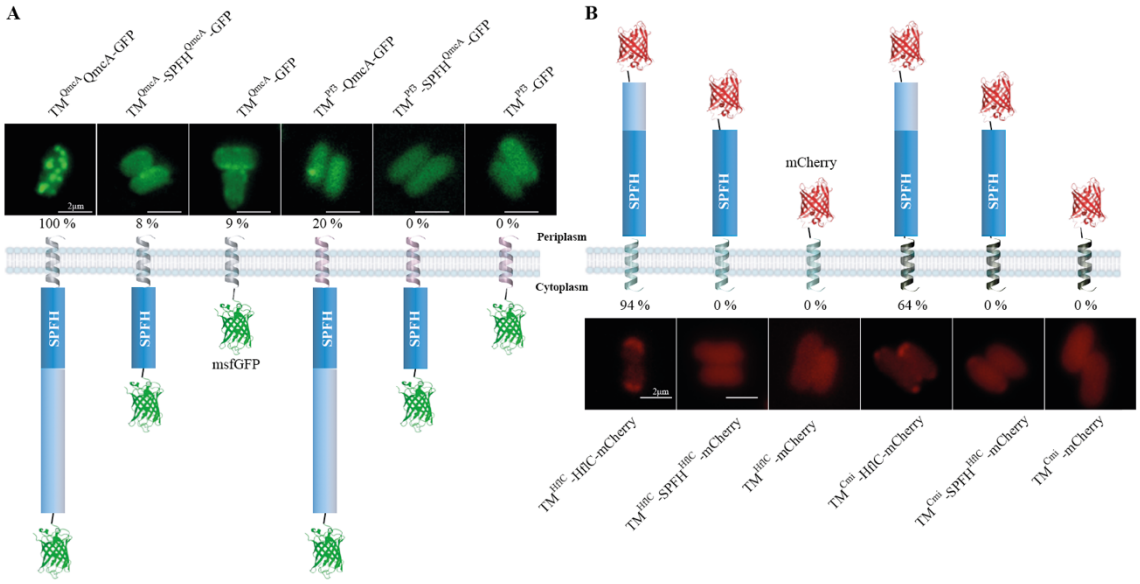

Figure 3. The localization pattern and membrane topology of full-length, domain swapped or truncated versions of QmcA and HflC. (**A**) GFP fusion derivatives of QmcA and (**B**) mCherry fusion derivatives of HflC. The representative images are shown in each strain with the frequencies of cells showing punctate (**A**) or polar localization (**B**). In membrane topology, helical structures represent transmembrane (TM) domains; silver, native TM domain of QmcA; pink, Pf3 domain; green, native TM domain of HflC; black, Cmi domain. Scale bars are 2 μm.

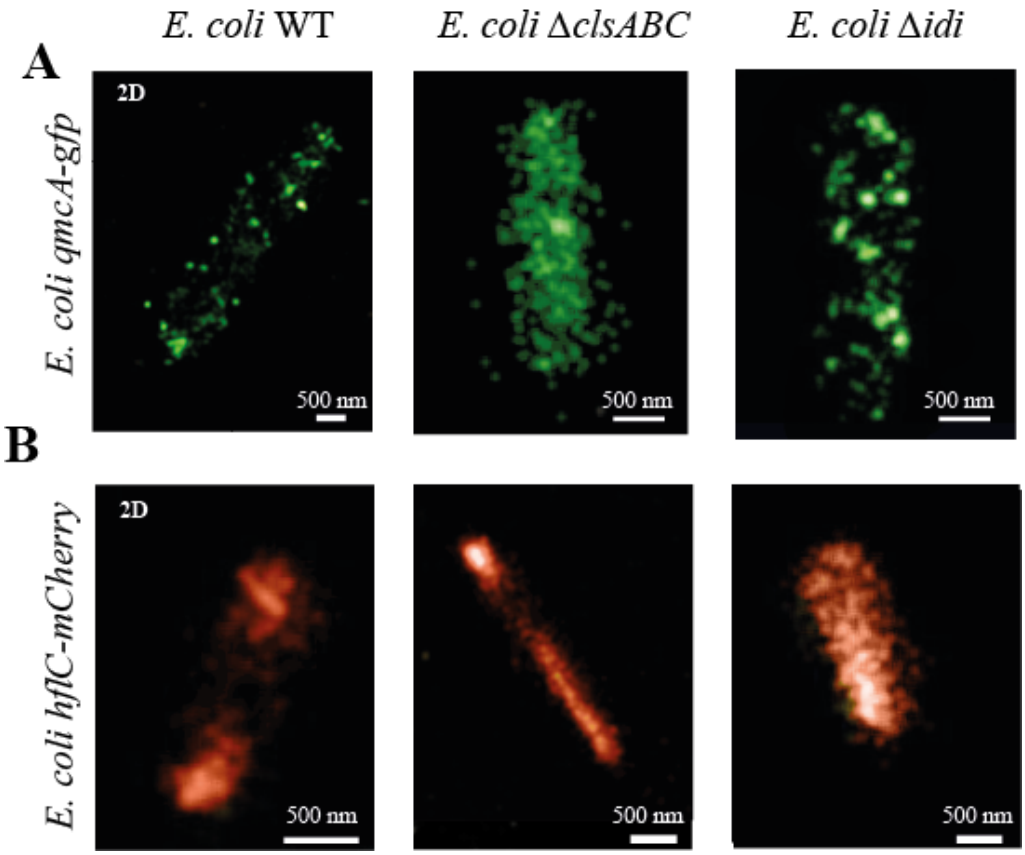

Figure 4. Alteration of QmcA and HflC cell localization in *E. coli* cardiolipin and isoprenoid pathway mutants. Two-dimensional super-resolution microscopy images of WT, Δ*clsABC*, and Δ*idi* strains expressing QmcA-GFP (**A**) and HflC-mCherry (**B**) in stationary phase.

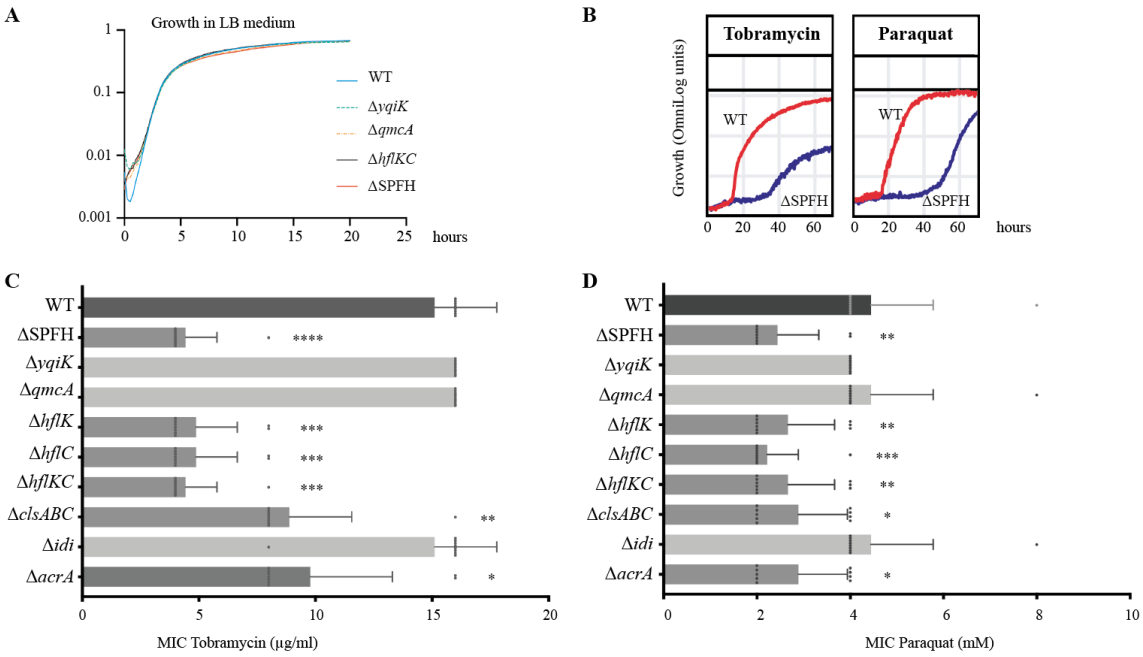

Figure 5. Phenotypic analysis of *E. coli* SPFH mutants. **A**: Bacterial growth curve of WT and SPFH gene deletion mutants in LB medium. **B**: Biolog bacterial growth curve of WT and ΔSPFH in the presence of tobramycin and paraquat. **C**: Minimum inhibitory concentration (MIC) for tobramycin of *E. coli* WT and indicated mutants. **D**: Minimum inhibitory concentration (MIC) for paraquat of *E. coli* WT and indicated mutants. *$p < 0.05$, **$p < 0.01$, ***$p < 0.001$, ***$p < 0.0001$ compared with WT.

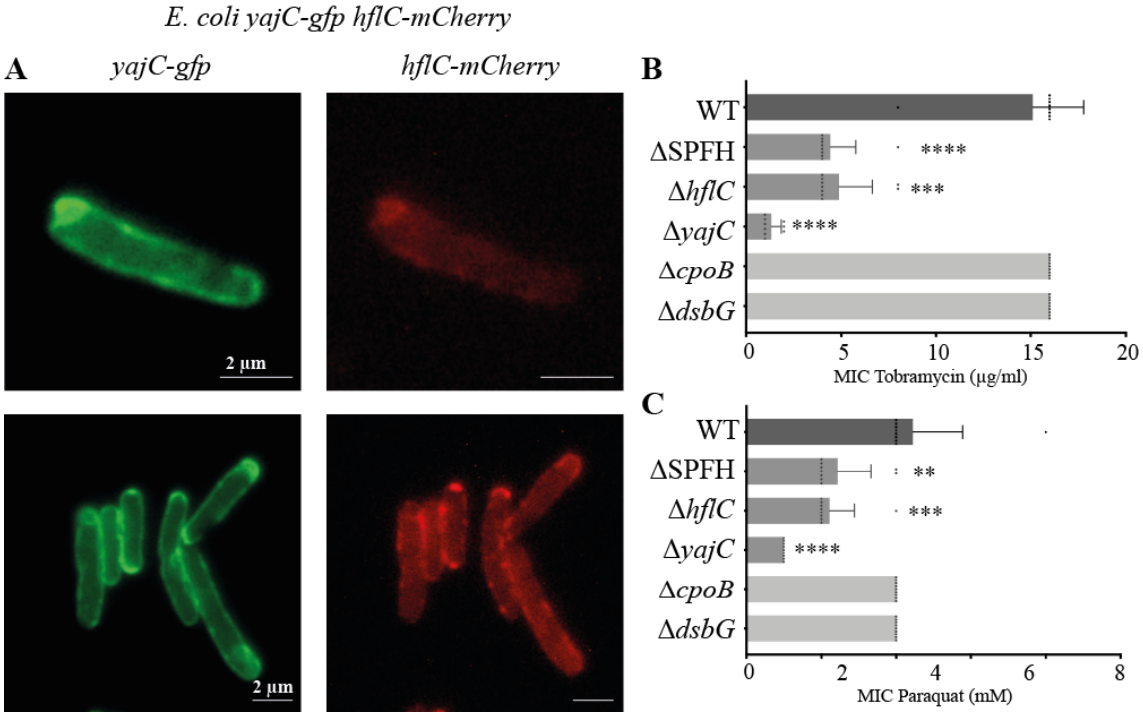

Figure 6. Localization of YajC-GFP and susceptibility of a Δ*yajC* mutant to tobramycin and paraquat. **A:** Epifluorescence microscopic images of cells expressing both YajC-GFP and HflC-mCherry in exponential phase with high and low magnifications. **B** and **C:** Minimum inhibitory concentration (MIC) for tobramycin (B) and paraquat (C) of *E. coli* WT and indicated mutants. WT, *ΔSPFH*, and *ΔhflC* strains are duplicated from Fig. 5C and D and presented here for the comparison. $^{**}p < 0.01$, $^{***}p < 0.001$, $^{****}p < 0.0001$ compared with WT.